Photoinduced Ultrafast Dynamics of Coumarin 343 Sensitized p-Type-Nanostructured NiO Films

Ana Morandeira, Gerrit Boschloo,† Anders Hagfeldt,† and Leif Hammarström*

Department of Physical Chemistry, Uppsala University, Box 579, SE-751 23 Uppsala, Sweden

Received: June 15, 2005

Photoinduced electron transfer from the valence band of nanocrystalline NiO, a p-type semiconductor, to an excited bound dye, coumarin 343, and the subsequent recombination have been measured by femtosecond transient absorbance spectroscopy probing with white light. It was found that both processes are nonexponential. The photoinduced electron transfer from the semiconductor to the excited bound dye has an ultrafast component (∼200 fs), which is comparable to the time constants measured for photoinduced electron injection in C343−TiO_2 colloid solutions. The process is very efficient and constitutes the main path of deactivation of the excited dye. Back electron transfer is also remarkably fast, with the main part of the recombination process happening with a time constant of ∼20 ps. Dye-sensitized nanostructured p-type semiconductors are attractive materials due to their potential use as photocathodes in dye-sensitized solar cells and solid electrolytes in solid-state dye-sensitized solar cells. To our knowledge, this is the first time that the photoinduced electron-transfer kinetics of a sensitized p-type semiconductor has been studied.

1. Introduction

The development of dye-sensitized photoelectrochemical solar cells (DSSCs) is a very active research field due to the promising application of these systems as low-cost alternatives to conventional solid-state devices.[1] Common DSSCs are based on wide band-gap n-type metal oxide semiconductors sensitized to visible light by dye molecules. The photocurrent is produced by the injection of an electron from the excited dye to the conduction band of the semiconductor. To regenerate the initial system and to avoid back electron transfer from the semiconductor to the oxidized dye, the latter is reduced to its original state by electron transfer from a suitable redox electrolyte. The injected electron in the conduction band diffuses to the back contact. The oxidized electrolyte is regenerated at the counter electrode, and the cycle is closed. The current systems are quite efficient, with DSSCs based on nanostructured TiO_2 sensitized with a ruthenium complex (Grätzel cells) having achieved solar energy conversion efficiencies over 10%.[2]

A common feature of DSSC and other dye-sensitized solid systems (halides in photography, for instance) is that the excited sensitizer works as electron donor. DSSCs have been optimized to work with a photoactive anode (the sensitized n-type semiconductor) while the cathode remains "passive". However, DSSCs where the cathode is photoactive are possible[3−5] and the development of photocathodes (sensitized p-type semiconductors) can open the possibility of production of DSSCs in which both electrodes are photoactive, forming a tandem cell. This is a very attractive perspective, as already pointed out by He et al.[3] While the theoretical upper limit of solar energy conversion efficiency for a cell with only one photoactive electrode is ∼30%, the corresponding limit for a device with two photoactive electrodes is ∼43%. Therefore, the production of DSSCs with two photoactive electrodes where the energy levels and band gaps of sensitizers and semiconductors have been optimized could provide a new way to significantly improve the conversion efficiency of DSSCs. However, so far, the efficiency of such cells has been very low when compared to the well-known Grätzel cell. A better understanding of the mechanism of production of cathodic photocurrent could help to improve its efficiency. Another important reason for improving our understanding of photoinduced electron transfer in sensitized p-type semiconductors is the development of solid-state electrolytes in solid-state DSSCs.[6−8]

While there are previous studies on the photoelectrochemistry and photophysics of sensitized p-type semiconductors,[9,10] this paper is, to our knowledge, the first study of the dynamics of photoinduced electron transfer from a p-type semiconductor to an excited bound dye (see Figure 1A). As semiconductor, we used nanostructured NiO, a wide band-gap p-type semiconductor, which has already been used for DSSCs[3,4] and for which the spectroelectrochemistry has been described in detail in ref 11. As sensitizer we chose coumarin 343 (see Figure 1B). This organic laser dye is suitable from an energetic point of view and it has already been used with success in the sensitization of nanostructured TiO_2 [12−17] and ZnO.[18] From the redox and excited-state energy data in Figure 1B, one may estimate a driving force for electron transfer to excited coumarin, $\Delta G° \approx -1.0$ eV, and an even larger value for recombination of the reduced bound dye and oxidized NiO, $\Delta G° \approx -1.6$ eV. Coumarin 343 sensitized NiO was chosen as a model system to study interfacial electron-transfer dynamics in dye-sensitized p-type semiconductors, as a prelude to a collaborative study with Dr. Fabrice Odobel, University of Nantes, on this topic.

2. Experimental Section

2.1. Samples. Nanostructured NiO films were prepared on microscope glass (Menzelglass) according to the procedure described in ref 11. The films were 1−3 μm thick and gray. The color of the films was attributed to partial oxidation of the

* To whom correspondence should be addressed. E-mail: Leifh@fki.uu.se.
† Present address: Department of Chemistry, Royal Institute of Technology (KTH), Teknikringen 30, SE-10044 Stockholm, Sweden.

10.1021/jp053230e CCC: $30.25
Published on Web 09/28/2005

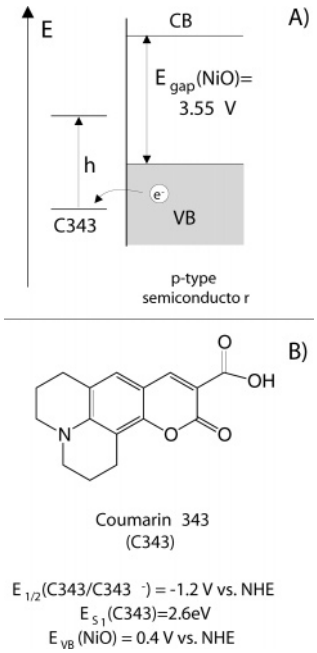

Figure 1. (A) Schematic representation of photoinduced electron transfer in a dye-sensitized p-type semiconductor. An electron is transferred from the valence band (VB) of the p-type semiconductor (NiO) to the excited dye (C343). Such a system can be used as active electrode, photocathode, in a DSSC. (B) Structure of coumarin 343 (C343) and some energy values: reduction potential of C343 in MeCN, $E_{1/2}$(C343/C343$^-$), energy of the first excited singlet state of C343 in MeCN (calculated from absorption and fluorescence spectra), E_{S_1}(C343), and valence band (VB) edge of nanostructured NiO measured in water at pH = 6.8, E_{VB}(NiO).

semiconductor during the sintering. Dye sensitization of the NiO films was carried out by soaking the film in an ethanol solution of coumarin 343 (5×10^{-4} M) overnight. The sensitized films were then rinsed with ethanol and dried at room temperature.

Coumarin 343 was purchased from Aldrich and was used as received for dye sensitization and for femtosecond transient absorbance measurements. For the flash-photolysis measurements, in which the signal was extremely weak, the measurements were carried out with both commercial and recrystallized (ethanol) coumarin 343. No significant differences were observed and the presence of impurities was discarded. Ethanol (Kemetyl), acetonitrile (Merck), triethanolamine (Merck), and acetic acid (Fluka) were of the highest commercially available purity and were used as such.

2.2. Steady-State Measurements. Absorption spectra were recorded on a Hewlett-Packard HP 8453. Fluorescence spectra were measured on a SPEX-Fluorolog fluorimeter. Fluorescence measurements of NiO and dye-sensitized NiO films were carried out in front-face geometry.

2.3. Femtosecond Transient Absorbance Measurements. 2.3.1. Setup. The femtosecond laser system consists of a 1 kHz regenerative amplifier (Quantronix) pumped by a Q-switched frequency doubled Nd:YLF laser (Quantronix) and seeded by a mode-locked Ti:sapphire oscillator (Mira, Coherent Radiation), the latter pumped by a continuous wave argon-ion laser (Coherent Radiation).

After compression, the fundamental output (800 nm) was split into a pump and a probe beam (70/30). The blue pump light at 422 nm was obtained by a sum frequency generation of the output of an optical parameter amplifier (TOPAS, Light Conversion Ltd). The IR output light, 1266 nm, traveled through a $\lambda/2$ plate and then through a BBO crystal (1 mm), where pulses of 636 nm were generated. Part of the 1266 nm light was delayed and mixed in a second BBO crystal (1 mm) with the 633 nm beam to obtain 422 nm pulses of energy between 0.4 and 0.8 μJ. Then, the 1 kHz pump passed a chopper in which every other pulse was blocked before it was focused in the sample.

The sample was mounted on a holder which moved up and down with a frequency of about 1 Hz. The probe beam was led through an optical delay line and focused on a moving CaF_2 plate where white light continuum (WL) was generated. A beam splitter was used to produce a WL reference beam. The probe and reference beams were focused through the slit of a monochromator and detected by two 512 pixel diode arrays of a detector system constructed by Dr. Torbjörn Pascher, Lund. The diode arrays were read once every laser pulse, and hence the transient absorption was calculated for two directly following pulses. All measurements were carried out at the magic angle.

The transient absorption spectra presented here are the average of 5−15 scans with 500−1500 shots at each time step, depending on the quality of the signal. The absorbance of the liquid samples was about 0.2 and that of the sensitized films about 1 at the excitation wavelength. The experiment response function, measured as the full width at half-maximum (fwhm) of a Gaussian pulse, was obtained from the data analysis (see below). On film samples, the fwhm was estimated to be about 170 fs at 360 nm, 150 fs at 450 nm, and 120 fs at 600 nm. Measurements on liquid samples (1 mm quartz cell) gave ∼20% larger fwhm values.

2.3.2. Data Analysis. The global analysis of the data was performed by a global analysis routine included in the software Igor Pro (Wavemetrics). Basically, the transient absorbance curve of every wavelength included in the analysis is reproduced by a Gaussian function convoluted to a variable number, *n*, of exponential functions. The routine optimizes simultaneously the *n* global decay time constants for every analyzed wavelength. Preexponential factors and width (response function) and center of the Gaussian (time zero) are characteristic of every probe wavelength.

To time correct our transient absorbance spectra from the WL chirp, the following procedure was carried out. From the above data analysis, time zero, $t_0(\lambda_{pr})$, the time at which a given probe wavelength overlaps with the pump beam in the sample, was obtained. Then, $t_0(\lambda_{pr})$ was plotted versus λ_{pr} and fitted to a polynomial function. Finally, the obtained polynomial function was used in a Matlab home-written routine to time correct the measured transient absorbance spectra.

2.4. Nanosecond and Microsecond Flash-Photolysis Measurements. Nano- and microsecond transient absorption experiments were obtained with a flash-photolysis setup consisting of a Nd:YAG laser/optical parametric oscillator (OPO) combination (Quantel/Opotek) and a flash-photolysis spectrometer (Applied Photophysics). The analyzing light and the laser beam overlapped in the sample in a 90° cross beam configuration. The samples were excited at 450 nm with 5 ns pulses of 35 mJ in a 1 cm quartz cell. At least 10 shots were averaged for each curve.

3. Results and Discussion

3.1. Steady-State Measurements. To obtain a clear picture of the behavior of coumarin 343 sensitized NiO, it is crucial to

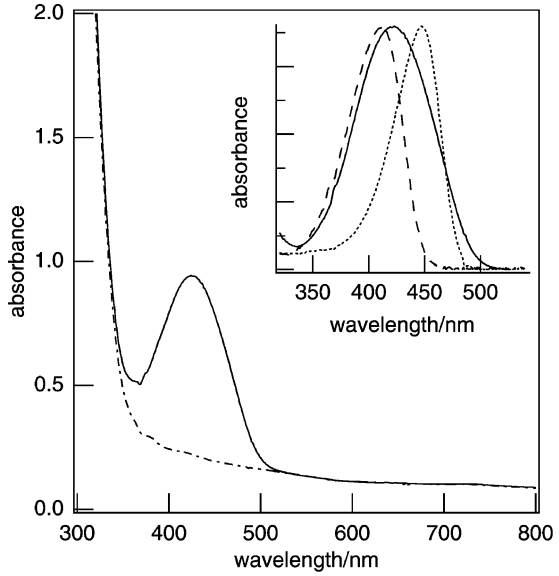

Figure 2. Steady-state absorption spectra of C343|NiO (solid line) and NiO (dash−dot line). Inset: Steady-state absorption spectra of C343|NiO (solid line, NiO absorption has been subtracted), C343H (dotted line, the solvent is MeCN), and $C343^-$ (dashed line, the solvent is EtOH saturated with Na_2CO_3).

know and understand the behavior of the dye in solution. Coumarin 343 is a carboxylic acid and therefore it is commonly found in solution as a mixture of the neutral and anionic forms. Consequently, in addition to the study of the dye-sensitized NiO, we carried out reference measurements on both the neutral and anionic forms of the dye in solution. Hereafter, for the sake of clarity, when we generically refer to the dye we will use the term C343. When we specifically refer to the neutral and anionic forms, we will use the terms C343H and $C343^-$, respectively. Finally, when we will refer to coumarin 343 sensitized NiO, we will use the term C343|NiO.

To characterize C343H, we carried out absorbance and fluorescence measurements in MeCN and in slightly acidic EtOH (∼1% v/v of acetic acid). The spectra in the visible region were very similar in both solvents. C343H in MeCN presents absorbance and fluorescence maxima at 447 and 491 nm, respectively (446 and 488 nm in acidic EtOH). On the other hand, $C343^-$ was characterized in $N(EtOH)_3$ and basic EtOH (EtOH saturated with Na_2CO_3). Again, similar values for the absorption and fluorescence peaks, 412 and 473 nm respectively, were found in the two solvents. In both C343H and $C343^-$, the bands were broad and structureless.

C343|NiO presents an absorption maximum around 422 nm, between the absorption maxima of $C343^-$ and C343H (see Figure 2). The position of the band can shift slightly, up to 5 nm, depending on the conditions of sensitization (dye concentration and duration of sensitization). The main difference with the absorption bands of the dye in solution is that the band is significantly broader. Broadening of the absorption band of the dye upon binding has already been observed in coumarin-sensitized TiO_2, and it is commonly attributed to the coupling of the dye with the semiconductor. Another plausible reason for the broadening would be the presence of several binding sites or modes of the dye to the semiconductor. This hypothesis can be supported by the small shifts observed in the absorbance peak depending on the sensitization conditions. A combination of both effects is likely, but no further investigation on the subject was carried out in this work.

The fluorescence from the bound dye is red-shifted and appears to be strongly quenched when compared to the emission

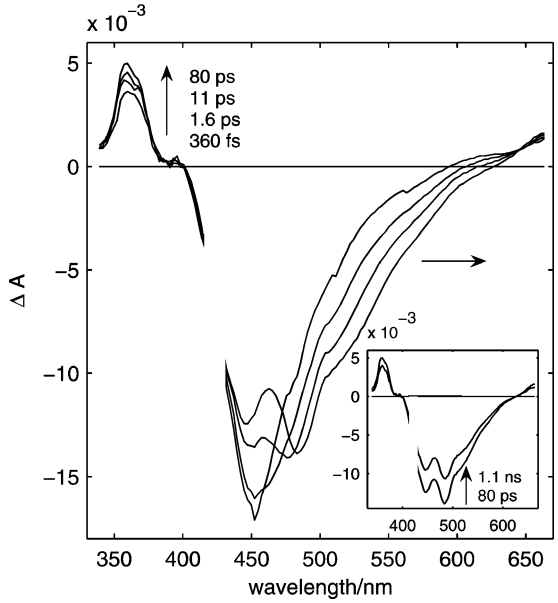

Figure 3. Transient absorption spectra of C343H in EtOH (1% of acetic acid) at different times after excitation (λ_{exc} = 422 nm; the spectrum in the pump region is omitted due to the Rayleigh scattering). For a short time after excitation the GB and the SE bands overlap. At longer times, the SE red shifts and the two bands become clearly distinct. Inset: After 80 ps the shape of the transient absorption spectrum remains constant. At 1.1 ns the decay of the excited state is noticeable.

from C343H and $C343^-$. Even though quantification of the fluorescence from films is difficult, the quenching must be very significant. C343 has a very high fluorescence efficiency in both neutral and deprotonated forms,[19,20] but the observed fluorescence from C343|NiO is in the same order of magnitude as the Raman scattering from the NiO film.

3.2. Time-Resolved Measurements

3.2.1. C343 in Acidic EtOH. Figure 3 shows the transient absorption spectrum of C343H in EtOH/acetic acid (99:1) at different times after excitation (λ_{exc} = 422 nm). Shortly after excitation (t = 360 fs), the spectrum consists of three bands. There are two positive bands which can be atributted to excited-state absorbance (ESA) transitions from C343H*. There is a well-defined ESA band with maximum at 360 nm, and it is possible to observe part of another ESA band above 595 nm. Between the two ESA bands there is a strong, sharp negative band with maximum bleach at 452 nm. This negative band is a combination of ground-state bleach (GB) (λ_{max}(C343H) = 446 nm, see inset in Figure 2) and stimulated emission (SE) from the unrelaxed excited coumarin. Two isosbestic points are present at 400 and 595 nm.

Later transient absorbance spectra at t = 1.6, 11, and 80 ps show how the negative band broadens asymmetrically toward the red, until it is split in two bands. The band in the blue can be clearly assigned to GB (λ_{max}(GB) ∼ 446 nm). The negative band in the red is due to SE. The shift of the SE band toward the red is due to the fluorescence Stokes shift that is commonly observed in coumarin derivatives.[21] At the same time, the ESA band at 360 nm grows. The isosbestic point at 400 nm remains constant. The isosbestic point at 600 nm shifts to the red (627 nm), in agreement with the Stokes shift of the SE, and a new isosbestic point appears around 645 nm.

Finally, if we compare the traces at 80 ps and 1.1 ns (Figure 3, inset), we can observe that the shape of the spectrum is the same (λ_{max}(ESA) ∼ 485 nm, very close to the 488 nm from

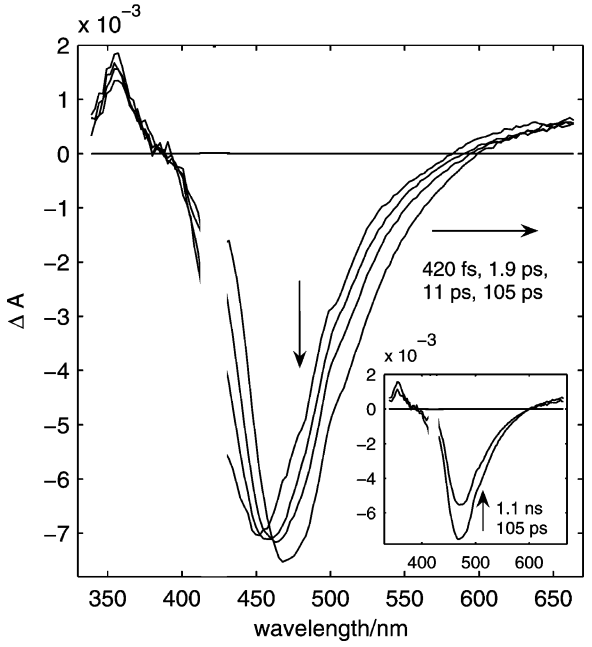

Figure 4. Transient absorption spectra of $C343^-$ in EtOH (saturated with Na_2CO_3) at different times after excitation ($\lambda_{exc} = 422$ nm). The main feature is that the SE band shifts to the red and increases in intensity with time. Inset: After 105 ps the shape of the transient absorption spectrum remains constant. At 1.1 ns the decay of the excited state is noticeable.

steady-state fluorescence measurements). However, at 1.1 ns, the decay of C343H* is already noticeable.

A four exponential function is required to reproduce the data in a global analysis of the kinetics at 460 nm (blue edge of the steady-state emission band), 490 nm (maximum of the steady-state emission band), and 540 nm (red edge of the steady-state emission band). The time constants are 3.75 ns, 28 ps, 3 ps, and an ultrafast component in the range of 100−300 fs. The long time constant is due to the decay of the singlet excited state which it is typically in the order of a few nanoseconds for 7-aminocoumarin derivatives.[18,22] The other three time constants are due to the dynamic Stokes shift of the emission. Since the dipole moment of coumarins changes significantly upon excitation, the dynamic Stokes shift of their emission is usually attributed to solvation dynamics and coumarin derivatives are common probes in the study of liquid dynamics.[21] Typical measurements of liquid dynamics consist of monitoring the fluorescence kinetics of a probe in a given solvent at different emission wavelengths by fluorescence up-conversion. From the various single wavelength kinetics curve, it is possible to reconstruct the evolution of the emission spectrum with time and obtain a spectral response function. From such a procedure, the solvation time constants of coumarin 153 (another rigid 7-aminocoumarin) in EtOH have been obtained (29.6 ps, 5.03 ps, 390 fs, and 30 fs).[22] Despite the different experimental and analysis techniques, these values are in good agreement with the time constants of the dynamical Stokes shift that we measured for C343H in EtOH (28 ps, 3 ps, and 100−300 fs). The kinetics of the 30 fs time constant is too fast to be detected by our setup.

3.2.2. C343 in Basic EtOH. Figure 4 shows the transient absorption spectrum of $C343^-$ in Na_2CO_3 saturated EtOH at different times after excitation ($\lambda_{exc} = 422$ nm). As in the case of C343H above, three bands are present in the spectrum shortly after excitation ($t = 420$ fs). Again, there are two ESA bands. There is a well-defined ESA band at 355 nm and the blue part of another band above 582 nm. Continuing the similarity with C343H, there is a strong negative band with maximum at 450 nm. It is when interpreting this negative band that a significant difference with the transient absorbance spectrum of C343H at 360 fs arises. The absorbance maximum of $C343^-$ is at 412 nm. However, there is practically no GB appearing in this region. The closeness of the pump wavelength makes the analysis more difficult, but the lack of significant bleach in the region is, nevertheless, quite evident. This is a clear sign that there must be a strong ESA band in the same region which is almost canceling the GB. This interpretation is reinforced by the fact that a strong ESA band in that region has also been observed in the case of coumarin 153[23] (another rigid 7-aminocoumarin). The observed negative band centered at 450 nm must then be mostly due to SE from the unrelaxed $C343^{-}$*. The two isosbestic points are at 383 and 582 nm.

At later times it is observed that the SE band of $C343^-$ shifts to the red, as in the case of C343H, and increases in intensity. The increase of SE intensity with time can be attributed to a smaller overlap with the "hidden" ESA band in the bleach region. Since the SE is shifting to the red with time, the overlap decreases and therefore the SE band becomes more negative. Meanwhile, the transient absorption in the bleach region becomes less negative (see spectral region between 400 and 450 nm in Figure 4). Even though the SE band shifts, no GB band "appears", as was seen for C343H, presumably due to the compensating ESA. On the other hand, the intensity of the ESA band at 355 nm increases significantly from 460 fs to 1.9 ps. It decreases slightly from 1.9 to 11 ps and thereafter, from 11 to 105 ps, remains practically constant.

The inset of Figure 4 shows a comparison of the transient absorbance spectra at 105 ps and 1.1 ns. The shape is very similar. In both traces the SE band is centered around 473 nm, which agrees perfectly with the value from steady-state fluorescence. However, at 1.1 ns the decay of $C343^{-}$* is already noticeable. The isosbestic point around 383 nm remains constant during the temporal evolution of the transient absorbance spectrum, but the other one shifts to the red to a final value around 610 nm.

As in the case of the neutral form, a four exponential function is required to reproduce the data in a global analysis of the kinetics at 450 nm (blue edge of the steady-state emission band), 470 nm (maximum of the steady-state emission band), and 520 nm (red edge of the steady-state emission band). The time constants are 3.3 ns, 60 ps, 13 ps, and 1.1 ps. Again, the long time constant is due to the decay of the singlet excited state. The other three time constants are due to the dynamic Stokes shift of the emission. The fast components are in good agreement with the solvation time constants of C343 in MeONa−MeOH (basic methanolic solution) reported by Tominaga et al.,[24] 1.0 and 10.3 ps, and measured by fluorescence up-conversion. The fact that the solvation dynamics of $C343^-$ is somewhat slower than that of the neutral form is not unexpected. The necessary addition of Na_2CO_3 to obtain the anionic form increases the viscosity of the solution and, therefore, slows down the diffusional components of the solvation. Moreover, the presence of electrolytes is known to slow solvation dynamics.[25−27]

3.2.3. C343 Sensitized NiO. Quenching of the Excited State and Formation of the Products. Figure 5A shows the temporal evolution of the transient absorption spectrum of C343|NiO during the first 5 ps after excitation ($\lambda_{exc} = 422$ nm). At a very short time after excitation, $t = 150$ fs, the transient absorbance spectrum of C343|NiO resembles very much that of $C343^{-}$* in solution (Figure 4). There are two ESA bands at 355 nm and

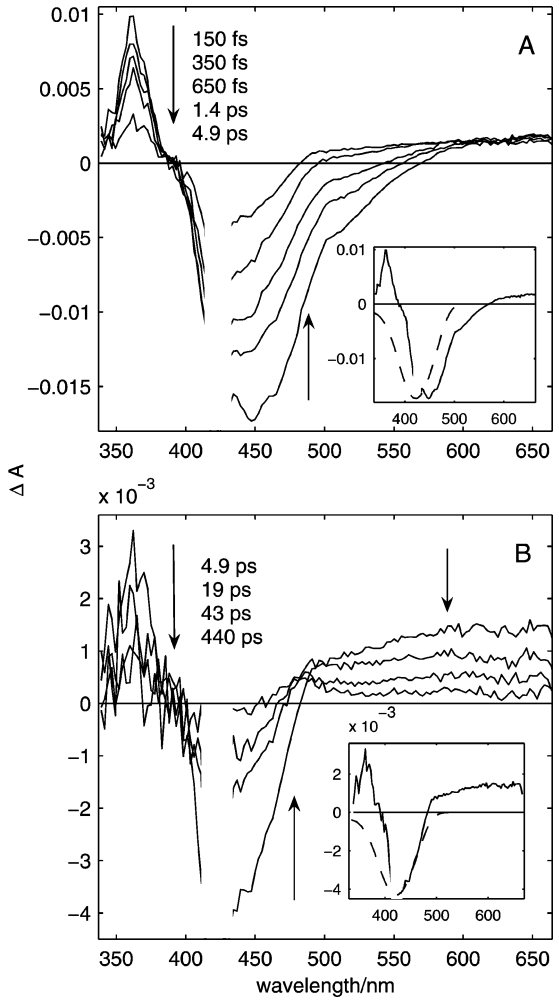

Figure 5. Transient absorption spectra of C343|NiO at different times after excitation ($\lambda_{exc} = 422$ nm). The inset in A presents a comparison between the GB band (dashed line) and the transient absorption spectrum at 150 fs after excitation (solid line). The inset in B presents a comparison between the GB band (dashed line) and the transient absorption spectrum at 4.9 s after excitation (solid line). In both cases the GB band was estimated from the steady-state absorption spectrum. The normalization factor is arbitrary and it has been chosen to facilitate the comparisons.

above 570 nm, there is a negative band which peaks at 448 nm, and the two isosbestic points are at 385 and 570 nm. The negative band is a combination of GB and unrelaxed SE and, as in the case of $C343^{-}$*, part of the bleach is "missing". This is clearly shown in the inset of Figure 5A, which presents a comparison between the GB band (estimated from the steady-state absorbance spectrum; the normalization factor is arbitrary and it has been chosen to facilitate the comparison) and the 150 fs transient absorbance spectrum. As commented above, this is an indication of a strong ESA which is canceling a significant part of the broad GB. The fact that the 150 fs transient spectrum of C343|NiO resembles more the early spectrum of $C343^{-}$* than that of C343H* seems to indicate that the dye deprotonates when binding to the semiconductor as expected.

The subsequent evolution of the transient absorbance spectrum of C343|NiO is very different to that of $C343^{-}$ and C343H in solution. During the first 5 ps, there is a dramatic quenching of the excited state of C343|NiO. This is shown by the decrease of the ESA band at 355 nm and by the recovery of the SE which leads to the formation of a positive band in the same wavelength region. The inset of Figure 5B shows a comparison between the GB band and the 4.9 ps transient absorbance spectra of C343|NiO. When the insets from parts A and B of Figure 5 are compared, it becomes evident that at 4.9 ps the SE has disappeared and that the remaining negative band must be due to GB. Therefore, we can safely assume that the observed positive bands at 4.9 ps belong to the photoproducts of the quenching process.

Identification of the Products. As mentioned in the Introduction, one of the main purposes in the design of C343|NiO is to produce a system where photoinduced electron transfer from a p-type semiconductor to the excited sensitizer occurs. If this is indeed the case, excitation of C343|NiO will lead to the formation of the radical anion of the bound dye and the oxidized semiconductor, to which we will refer as $C343^{\bullet -}$|NiO(+). The key question then is to see if the observed transient absorbance spectrum at 4.9 ps can be attributed to absorbance from $C343^{\bullet -}$|NiO(+) and GB from C343|NiO or if there are other species involved in the photoreaction.

First of all, no transient absorbance signal was observed in blank measurements with NiO film. Consequently, the monitored transient absorption is due to the sensitization of the film with C343.

Spectroelectrochemistry of NiO has been studied by Boschloo et al.[11] Oxidized NiO presents a very large, structureless absorption band, with a maximum at 345 nm ($\epsilon_{345} \sim 6900$ M^{-1} cm^{-1}) and a gradual decrease from 350 to 1100 nm.

A direct determination of the absorption spectrum of the radical anion of C343 was not successful. C343|NiO could not be studied with standard nanosecond flash photolysis since the sample photodegradated after a few shots under conditions where the $N_3|TiO_2$ system was sufficiently stable for measurements (pump energy is much higher in flash photolysis than in the femtosecond transient absorbance measurements). Common spectroelectrochemistry measurements where not feasible due to the nonreversible reduction of C343, as observed in the cyclic voltammogram and already reported by Murakoshi et al.[18] To our knowledge, there are only two reports on the absorbance spectra of the radical anion of coumarin[28] or coumarin derivatives.[29] In the latter report, by Nad et al., the radical anions of six 7-aminocoumarins (including coumarin 153 which has the same rigid amino substituent as C343) were studied by pulse radiolysis in the spectral range from 450 to 800 nm. All the radical anions presented rather similar absorbance spectra, consisting of a broad band in the 500−800 nm region with two not very pronounced maxima around 600 and 700 nm ($\epsilon_{max} \sim 4000$ M^{-1} cm^{-1}). Qualitatively, this result agrees very well with the radical anion absorbance spectrum of coumarin reported by Shida[28] and measured at low-temperature MTHF matrix. The latter species also has a broad absorption band in the 500−800 nm region with maximum at 648 nm ($\epsilon_{648} \sim 3000$ M^{-1} cm^{-1}). Moreover, the radical anion of coumarin presents a stronger absorbance band in the near-UV with maxima at 410 ($\epsilon_{410} \sim 19000$ M^{-1} cm^{-1}) and 382 nm ($\epsilon_{382} \sim 12000$ M^{-1} cm^{-1}). From the above data it seems reasonable to assume that the absorbance spectrum of $C343^{\bullet -}$ presents a weak, broad band in the 500−800 nm region ($\epsilon_{max} \sim 4000$ M^{-1} cm^{-1}) and another, stronger band in the near-UV region (ϵ_{max} around 10000−20000 M^{-1} cm^{-1}).

The combination of the above-described features of oxidized NiO and $C343^{\bullet -}$ absorption spectra agrees qualitatively well with the observed transient absorbance spectrum of C343|NiO at 4.9 ps (see Figure 5). The broad, almost shapeless band observed to the red of the bleach band can be attributed to the mix of the similarly weak, shapeless bands of oxidized NiO and radical anions of 7-aminocoumarins in this region. To the

blue of the bleach band, the oxidized NiO presents again a rather shapeless, weak absorbance. The relatively well-defined band around 355 nm and, very especially, the fact that part of the strong GB band is "missing" (see inset in Figure 5B) could be attributed to a stronger near-UV band of $C343^{\bullet-}$. An approximate spectral decomposition of the transient absorbance spectrum at 4.9 ps as the sum of the spectra of oxidized NiO, GB bleach of C343, and radical anion of coumarin/coumarin 153 (from refs 11, 28, and 29, respectively) is presented in the Supporting Information.

Decay of the Products. Figure 5B presents the temporal evolution of the transient absorption spectrum after 4.9 ps. The spectra at 4.9, 19, and 43 ps present a similar shape, but already at 19 ps it is evident that the bands attributed to $C343^{\bullet-}|NiO(+)$ are decreasing and the GB is recovering. The straightforward interpretation is that back electron transfer from the reduced dye to the oxidized semiconductor is occurring and the initial system is regenerated.

The transient absorbance spectrum at 440 ps deserves a special comment. At this time, the remaining signal is extremely weak and almost all the GB has recovered. Nevertheless, it is possible to appreciate a positive band with maximum at 485 nm which is quite different from that of $C343^{\bullet-}|NiO(+)$. Flash-photolysis measurements of C343 in MeCN showed the presence of a very weak signal in the microsecond time scale (see Figure 7). Despite the weakness of the signal, the GB band of C343H (neutral form, $\lambda_{abs}^{max} = 447$ nm) and two positive bands with maxima around 370 and 490 nm can be discerned without ambiguity. Since the singlet excited state of C343 decays with a lifetime of ~4 ns, we attribute the positive transient bands to triplet−triplet absorption from C343. Due to the similarity between the flash-photolysis spectrum at 1.5 μs of C343 in MeCN and the transient absorbance spectrum at 440 ps of C343|NiO, we interpret the latter as triplet−triplet absorption from the bound dye. Therefore, this spectrum must correspond to a small subpopulation of sensitizer which undergoes a fast intersystem crossing and which relaxes in a much longer time scale. This point will be brought up again in the analysis of the kinetics.

Analysis of the Kinetics. To quantify and obtain a more detailed understanding of the dynamics of C343|NiO upon excitation, a global analysis of the kinetics was carried out. The conclusions obtained from the kinetics analysis, as we are going to show below, are in very good agreement with those obtained from the careful inspection of the spectral changes described in the former sections.

Not surprisingly, given the complexity of the dynamics, a four-exponential function is required to reproduce simultaneously 24 experimental curves. The time constants obtained from the global fit procedure are 210 fs, 2 ps, 23 ps, and a very weak component of 2 ns. Figure 6 presents the transient absorbance kinetics and best global fits of C343|NiO at two key wavelengths, 470 and 570 nm. Kinetics of $C343^-$ and C343H in solution are also shown for comparison. The chosen wavelengths are especially relevant for the interpretation of the data. Regardless of whether the dye is in its basic, neutral, or bound form, the signal at 470 nm is dominated by SE. Therefore, according to the amplitudes at 470 nm obtained by the global analysis, over 60% of the excited state is quenched with a time constant of 210 fs and about 30% is quenched with a time constant of 2 ps. At 570 nm, on the other hand, the transient absorbance spectrum of C343|NiO at 150 fs has an isosbestic point ($\Delta A = 0$) (Figure 5 A). In solution, the observed signal in this region is also very weak and the monitored dynamics is due to the Stokes shift of the SE band. Consequently, since SE in the bound dye is efficiently quenched on a subpicosecond time scale, the observed signal at 570 nm can be entirely

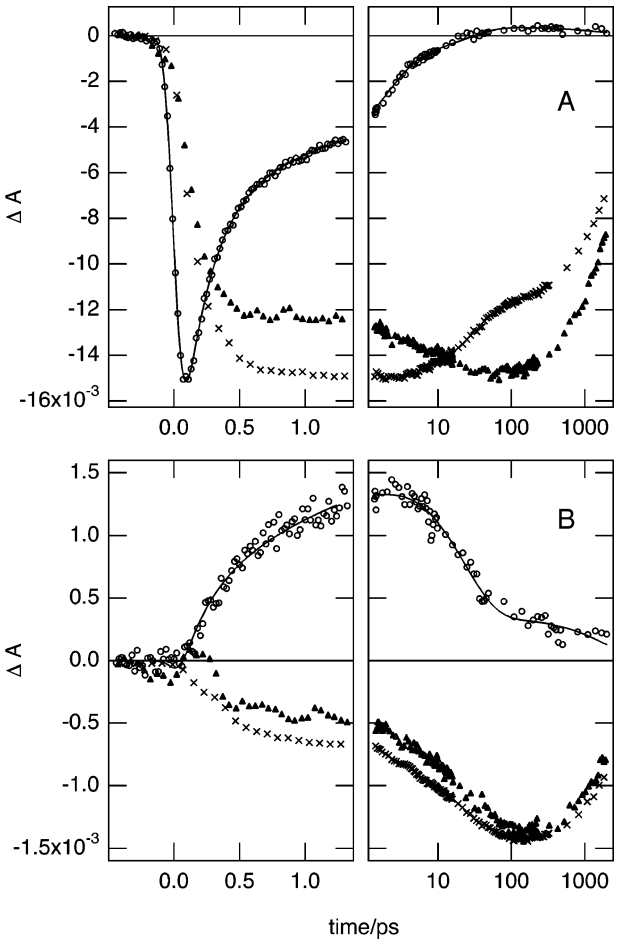

Figure 6. Transient absorption kinetics of C343|NiO (circles), C343H in EtOH (1% of acetic acid; crosses) and $C343^-$ in EtOH (saturated of Na_2CO_3; solid triangles) at (A) 470 nm and (B) 570 nm. The excitation wavelength is 422 nm. In the left part of the figure the scale is linear while in the right part it is logarithmic. For clarity, the transient absorption data from solution measurements has been normalized to the maximum absolute value of the film transient absorption curves.

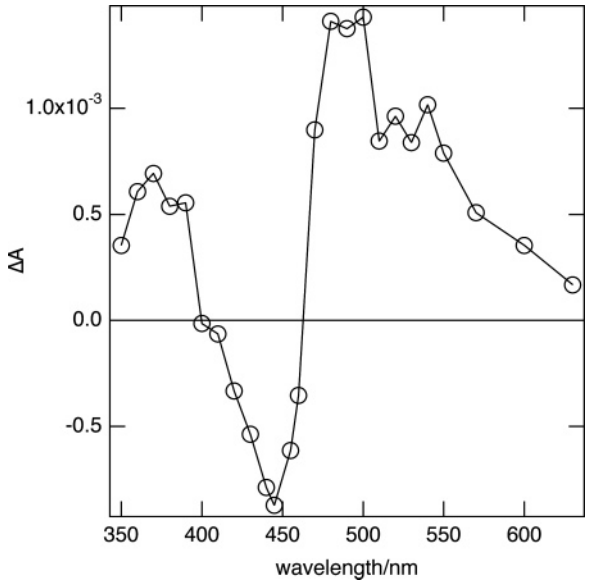

Figure 7. Flash-photolysis spectrum of C343H in MeCN at 1.5 μs after excitation ($\lambda_{exc} = 450$ nm).

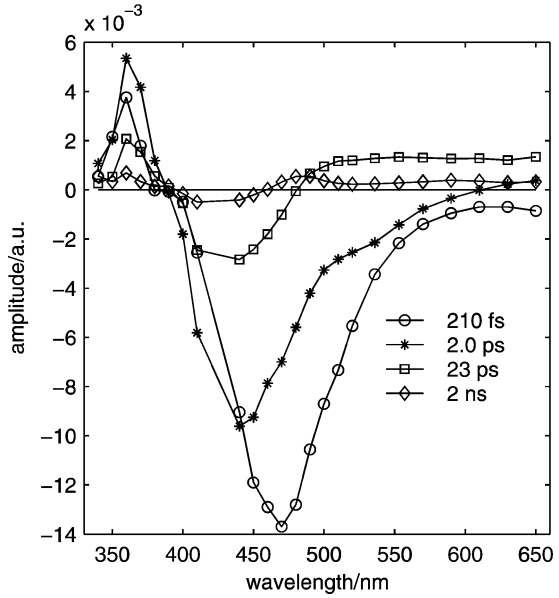

Figure 8. Plot of the preexponential factors obtained in the global fit analysis vs probe wavelength at each time constant (decay related spectra) for C343|NiO. See text for more details.

attributed to absorbance from the product. The preexponential factors obtained from the kinetic analysis showed that 65% of the product signal at 570 nm rises with a time constant of 210 fs and 35% rises with a time constant of 2 ps. This is in good agreement with the SE quenching. The main part of the product subsequent decay (80%) occurs with a time constant of 23 ps, while the small remaining fraction decays on a much longer time scale with a time constant of 2 ns.

A more detailed analysis of the kinetics can be done with a plot of the decay-related spectra from the global analysis of the kinetics. For a given time component, a plot of the preexponential factor versus probe wavelength (a decay-related spectrum) provides a very good picture of the species evolving at this time scale. In such a spectrum, a negative value means that a new species absorption is arising and/or GB is recovering and/or SE is being quenched. On the other hand, a positive value means that a species is decaying and/or a rise of SE. Figure 8 presents the four decay-related spectra obtained from the global analysis. The spectrum at 210 fs has a positive band around 360 nm (quenching of the ESA), a strong negative band at 470 nm (quenching of SE; it is so strong that it will hide the rise of a new species in the same region), and a negative tail above 600 nm (rise of C343$^{\bullet-}$|NiO(+)). At 23 ps, there is again, a somewhat larger positive band around 360 nm (decay of C343$^{\bullet-}$|NiO(+)), a negative band with maximum in the pump region (recovery of the GB), and a large, shapeless positive band in the red (again, decay of C343$^{\bullet-}$|NiO(+)). The decay-related spectrum at 2 ps shows mixed features between those of the spectrum at 210 fs and that at 23 ps. This is particularly evident in the position of the negative band, which it is placed between the SE and GB bands, with a maximum around 440 nm. Finally, in the spectrum at 2 ns, even though the amplitudes are very small, it is possible to distinguish two positive bands, one in the near-UV and the other in the visible with maximum around 485 nm, and a bleach band. As already mentioned in the former section, this spectrum is nearly identical to that of the triplet of C343 in MeCN (see Figure 7) and, therefore, it can be attributed to the decay of the triplet state of the bound dye. The enhanced triplet formation (compared to solution) could be due to paramagnetic centers in NiO. It is not clear if the triplet is formed from the initial singlet excited state or from recombination of the C343$^{\bullet-}$|NiO(+) state. As the singlet−triplet energy difference for similar coumarins is ∼1 eV,[30,31] the triplet and C343$^{\bullet-}$|NiO(+) states would be at similar energies, according to our estimate. Thus, we cannot on energetic grounds discriminate between the possible formation pathways. However, it is clear that this pathway only concerns a very small part of the population of excited C343|NiO, and consequently, it will be omitted from the rest of the discussion and conclusions.

From the analysis of the decay-related spectra it can be concluded that the time constant of 210 fs is linked to the photoinduced electron transfer from the semiconductor to the dye, while the time constant of 23 ps is linked to the back electron transfer. The fact that the spectrum at 2 ps presents mixed features highlights the complexity of the dynamics and can be interpreted as a sign that both photoinduced electron transfer and recombination also occur (and coexist) at this time scale. This is not surprising if it is considered that heterogeneous electron transfer is often described as multiphasic, stretching over several orders of magnitude[15,32] (and references therein), and that highly nonexponential dynamics can often be well reproduced with biexponential functions.

Comparison with C343 Sensitized TiO_2. Since, to our knowledge, there are no other ultrafast measurements on the dynamics of dye-sensitized p-type semiconductors, it is useful to take a look to the previous reports on C343-sensitized n-type semiconductors, particularly in the much studied TiO_2, and see if the processes are comparable despite their fundamental differences. While in photoinduced interfacial electron transfer of dye-sensitized TiO_2 the electron is transferred from the excited sensitizer to the semiconductor, in the system presented here, C343|NiO, the electron is transferred from the semiconductor to the excited dye.

Several spectroscopic measurements on the femtosecond and picosecond time scales have been reported for the system C343 sensitized TiO_2.[13−15,33,34] In most cases the monitored system consisted of sensitized colloidal nanoparticles of TiO_2. Only in one case,[34] a comparison was done between colloidal nanoparticles and nanocrystalline thin film. The estimated driving force for the forward electron transfer and the subsequent recombination[35] were identical to the values we estimate for the C343|NiO system. Fluorescence up-conversion measurements[33] showed a biexponential decay of C343 fluorescence with time constants of ca. 200 fs (95%) and >5 ps (5%), which are in the same order of magnitude as the time constants we have measured in C343|NiO for the decay of the excited state (210 fs and 2 ps). Measurements with femtosecond infrared spectrocopy,[13] which allows direct monitoring of the rise of the injected electron, showed a rise time constant of ca. 125 fs followed by highly nonexponential recombination dynamics with time constants of 150 fs, 15 ps, and 300 ps. It is worth noting that any slower injection process of small amplitude will be easily missed with such a fast recombination process. A later report from the same group,[34] where nanoparticles of higher cristallinity (and thin films) were used, showed a similar rise time constant, but the recombination process was significantly slowed (180 ps, 37%, and ≫1 ns). This effect was attributed to the reduction of the number of trap states due to the higher crystallinity of the semiconductor. Finally, femtosecond transient absorption measurements probing with white light were also carried out,[15] together with a data analysis very similar to the one we have presented here (global fit analysis, assignment of the involved species by interpretation of the decay related spectra). Again, highly nonexponential dynamics are observed with time con-

stants of 500 fs, 3 ps, 84 ps, and 3 ns. The injection of the electron was thought to occur during the excitation of the sample (<100 fs), and the authors attributed the four observed time constants to the recombination process. In our opinion, however, the assignment of the 500 fs time constant is ambiguous due to the similarity that the transient absorbance bands of the excited state of C343 and those of the radical cation present (the same authors point out this difficulty in a former report[14]) and the further complication of the pump beam being in the same spectral region as the stimulated emission from the dye (λ_{exc} = 495 nm). Careful observation of the decay-related spectra presented in ref 15 reveals a negative signal in the 500 fs decay-related spectrum in the region from 525 to 550 nm. This negative signal, which it is not present in the later decay-related spectra of the system, can very well be due to stimulated emission. Therefore, we are inclined to think, that at least a fraction of the electron injection is occurring with a time constant >100 fs in that study.

The reported values for the time constants of photoinduced interfacial electron transfer in C343 sensitized TiO_2 summarized above, are on the same order of magnitude as the values we have measured for C343|NiO. However, when we take into account the preexponential factors, the photoinduced electron transfer is globally slower in NiO. On the other hand, recombination processes are highly nonexponential in both systems, but significantly faster in NiO. It has been shown that the preparation of the sample (degree of cristallinity) and the experimental conditions (excitation wavelength, pump intensity, environment) can affect the observed photoinduced electron injection and recombination time constants of dye-sensitized TiO_2[32,34,36,37] as much as the indicated differences between C343 sensitized TiO_2 and C343|NiO. Since it is logical to expect a similar behavior in dye-sensitized NiO, more detailed studies are needed before drawing more fundamental conclusions from the comparison of the systems.

4. Summary

The photoinduced electron transfer from a nanostructured wide band-gap p-type semiconductor, NiO, to an excited bound dye, C343, has been measured for the first time. The process is nonexponential with a major ultrafast component (~200 fs), which is on the same order of magnitude as the time constants measured for photoinduced electron injection in C343−TiO_2 colloid solutions. This presents nanostructured NiO as a good material to be used as photocathode in DSSCs. However, back electron transfer, which is also nonexponential, is remarkably fast, with the main part of the recombination process occurring with a time constant of ~20 ps. To be able to use nanostructured NiO as an efficient photocathode, it will be important to understand why the recombination is so fast and, if possible, to slow the process. Further investigation in this direction is currently performed.

Acknowledgment. We thank Leonard Csenki for preparation of the NiO films. We are grateful to Reiner Lomoth for assistance in the photoelectrochemistry study of coumarin 343. We thank Sascha Ott for help in the purification of the dye. We are also grateful to Jan Davidson and Emad Mukhtar for assistance with the femtosecond laser system and helpful discussions. This work was supported by the Swedish Foundation for Strategic Research, the Wallenberg Foundation, and the Swedish Research Council. L.H. acknowledges a Research Fellow Position from the Royal Swedish Academy of Sciences. A.H. and G.B. acknowledge funding from MISTRA and the Swedish Energy Agency.

Supporting Information Available: An approximate spectral decomposition of the transient absorbance spectrum of C343|NiO at 4.9 ps as the sum of the spectra of oxidized NiO (from ref 11), GB bleach of C343 and radical anion of coumarin (from ref 28)/coumarin 153 (from ref 29). This material is available free of charge via the Internet at http://pubs.acs.org.

References and Notes

(1) O'Regan, B.; Grätzel, M. *Nature* **1991**, *353*, 737.

(2) Grätzel, M. *J. Photochem. Photobiol., C* **2003**, *4*, 145.

(3) He, J.; Lindström.; Hagfeldt, A.; Lindquist, S. E. *Sol. Energy Mater. Sol. Cells* **2000**, *62*, 265.

(4) He, J.; Lindström, H.; Hagfeldt, A.; Lindquist, S.-E. *J. Phys. Chem. B* **1999**, *103*, 8940−8943.

(5) Fernando, C. A. N.; Kitagawa, A.; Suzuki, M.; Takahashi, K.; Komura, T. *Sol. Energy Mater. Sol. Cells* **1994**, *33*, 301−315.

(6) O'Regan, B.; Schwartz, D. T. *J. Appl. Phys.* **1996**, *80*, 4749−4754.

(7) Jayaweera, P. M.; Kumarasinghe, A. R.; Tennakone, K. *J. Photochem. Photobiol., A* **1999**, *126*, 111−115.

(8) Bandara, J.; Weerasinghe, H. *Sol. Energy Mater. Sol. Cells* **2005**, *85*, 385−390.

(9) Memming, R.; Tributsch, H. *J. Phys. Chem.* **1971**, *75*, 562−570.

(10) O'Regan, B.; Schwartz, D. T. *Chem. Matter.* **1995**, *7*, 1349−1354.

(11) Boschloo, G.; Hagfeldt, A. *J. Phys. Chem. B* **2001**, *105*, 3039.

(12) Enea, O.; Moser, J.; Grätzel, M. *J. Electroanal. Chem.* **1989**, *259*, 59.

(13) Ghosh, H. N.; Asbury, J. B.; Lian, T. *J. Phys. Chem. B* **1998**, *102*, 6482−6486.

(14) Wachtveitl, J.; Huber, R.; Spörlein, S.; Moser, J. E.; Grätzel, M. *J. Photoenerg.* **1999**, *1*, 153.

(15) Huber, R.; Moser, J. E.; Grätzel, M.; Wachtveitl, J. *Chem. Phys.* **2002**, *285*, 39.

(16) Ramakrishna, G.; Ghosh, H. *N. J. Phys. Chem. A* **2002**, *106*, 2545−2553.

(17) Hara, K.; Sato, T.; Katoh, R.; Furube, A.; Ohga, Y.; Shinpo, A. Suga, S.; Sayama, K.; Sugihara, H.; Arakawa, H. *J. Phys. Chem. B* **2003**, *107*, 597.

(18) Murakoshi, K.; Yanagida, S.; Capel, M.; Castner, E. W. J. In *Nanostructured Materials*: *Clusters*, *Composites and Thin Films*; ACS Symposium Series 679; American Chemical Society: Washington, DC, 1997; pp 221−238.

(19) Reynolds, G. A.; Drexhage, K. H. *Opt. Commun.* **1975**, *13*, 222.

(20) Drexhage, K. H.; Erikson, G. R.; Hawks, G. H.; Reynolds, G. A. *Opt. Commun.* **1975**, *15*, 399−403.

(21) Glasbeek, M.; Zhang, H. *Chem. Rev.* **2004**, *104*, 1929.

(22) Horng, M. L.; Gardecki, J. A.; Papazyan, A.; Maroncelli, M. *J. Phys. Chem.* **1995**, *99*, 17311−17337.

(23) Kovalenko, S. A.; Ruthmann, J.; Ernsting, N. P. *Chem. Phys. Lett.* **1997**, *271*, 40.

(24) Tominaga, K.; Walker, G. C. *J. Photochem. Photobiol., A* **1995**, *87*, 127−133.

(25) Chapman, C. F.; Maroncelli, M. *J. Phys. Chem.* **1991**, *95*, 9095−9114.

(26) Huppert, D.; Ittah, V.; Kosower, E. M. *Chem. Phys. Lett.* **1989**, *159*, 267−275.

(27) Ittah, V.; Huppert, D. *Chem. Phys. Lett.* **1990**, *173*, 496−502.

(28) Shida, T. *Electronic Absorption Spectra of Radical Ions*; Physical Sciences Data; Elsevier: Amsterdam, 1988.

(29) Nad, S.; Pal, H. *J. Phys. Chem. B* **2002**, *106*, 6823.

(30) Priyadarsini, K. I.; Naik, D. B.; Moorthy, P. N. *J. Photochem. Photobiol., A* **1989**, *46*, 239−246.

(31) Priyadarsini, K. I.; Naik, D. B.; Moorthy, P. N. *Chem. Phys. Lett.* **1989**, *157*, 525−530.

(32) Kallioinen, J.; Benkö, G.; Myllyperkiö, P.; Khriachtchev, L.; Skårman, B.; Wallenberg, R.; Tuomikoski, M.; Korppi-Tommola, J.; Sundström, V.; Yartsev, A. P. *J. Phys. Chem. B* **2004**, *108*, 6365−6373.

(33) Rehm, J. M.; McLendon, G. L.; Nagasawa, Y.; Yoshihara, K.; Moser, J.; Grätzel, M. *J. Phys. Chem.* **1996**, *100*, 9577−9578.

(34) Hao, E.; Anderson, N. A.; Asbury, J. B.; Lian, T. *J. Phys. Chem. B* **2002**, *106*, 10191−10198.

(35) Moser, J. E.; Grätzel, M. *Chem. Phys.* **1993**, *176*, 493−500.

(36) Haque, S. A.; Tachibana, Y.; Willis, R. L.; Moser, J. E.; Grätzel, M.; Klug, D. R.; Durrant, J. R. *J. Phys. Chem. B* **2000**, *104*, 538−547.

(37) Asbury, J. B.; Anderson, N. A.; Hao, E.; Ai, X.; Lian, T. *J. Phys. Chem. B* **2003**, *107*, 7376−7386.